Lawrence Berkeley National Laboratory

Title
ACCELERATOR PHYSICS EXPERIMENTS AT ALADDIN

Permalink
https://escholarship.org/uc/item/5b91q2dg

Author
Chattopadhyay, S.

Publication Date
1985-07-01

ACCELERATOR PHYSICS EXPERIMENTS AT ALADDIN*

S. Chattopadhyay, M. Cornacchia, A. Jackson, and M.S. Zisman

Lawrence Berkeley Laboratory
University of California
Berkeley, California 94720

July 1985

ACCELERATOR PHYSICS EXPERIMENTS AT ALADDIN*

S. Chattopadhyay, M. Cornacchia, A. Jackson, and M. S. Zisman

Lawrence Berkeley Laboratory
University of California
Berkeley, California 94720

I. Introduction

In this paper we describe the results of our experimental s dy of the Aladdin accelerator, a 1 GeV synchrotron light source located at the University of Wisconsin. The work reported here was carried out during the latter part of April, 1985 under the auspices of the Aladdin Upgrade Study, whose mission was to assess the problems with the existing Aladdin storage ring and recommend corrective action. Our other work for the Upgrade Study has already been described [1-3].

The primary purpose of our experimental onslaught was to investigate reported anomalies in the behavior of the linear lattice, particularly in the vertical plane. This information was felt to be crucial to give us confidence in the "paper studies" that were carried out to assess the expected performance of Aladdin with a proposed 800 MeV injector [1-3]. In particular, a good understanding of the linear optics is crucial for "modeling" the machine in order to design the new injection system, an effective closed-orbit correction and beam steering system, etc.

A second goal of our experimental program was to estimate the ring broadband impedance. This information is required in order to ascertain that the high-current performance of the accelerator will be acceptable (in

terms of instabilities) at 800-1000 MeV. Finally, we wished to make mea-
surements of the longitudinal and transverse beam emittance in order to
test our predictions [3] of large emittance growth at low energies due to
intrabeam scattering (IBS).

Prior to our experiments, a great deal of experimental work on the
Aladdin ring had already been carried out by the staff of the University of
Wisconsin Synchrotron Radiation Center (SRC) and, more recently, by
A. Hofmann and P. Morton from SLAC. It had been observed, for example, that
the horizontal lattice functions had the expected fourfold symmetry and that
they generally agreed with model predictions from the lattice code SYNCH;
this is shown in Fig. 1. In contrast, however, it was reported that the
vertical lattice functions had only a twofold symmetry rather than the ex-
pected fourfold symmetry, and this was a cause of some concern.

A preliminary experiment to measure the broadband impedance of the ring
had also been carried out [4], and yielded a value for $|Z/n|$ of about 17 ohms.
This value is higher than the estimate [5] of $|Z/n| = 6$ ohms used during the
Upgrade Study, but not so high as to substantially affect any of our pre-
vious conclusions. Insofar as the impedance estimate in Ref. 5 did not in-
clude the contributions from either the kicker magnets or the clearing elec-
trode striplines, the measured impedance value was not felt to be seriously
in disagreement with the estimate; nonetheless, it was recommended by those
responsible for the first experiment [4] that we repeat the measurement.

With regard to the emittance growth issue, the general feeling at Alad-
din was that the beam size changed as a function of energy in a manner con-
sistent with that predicted in Ref. 3. Unfortunately, there was no quanti-
tative information available. Because the low energy behavior of Aladdin is
a good model for other rings that may be designed with a low injection

energy, it was deemed worthwhile to try to assess the low energy emittance behavior in a more quantitative fashion in order to allow direct comparison with our accelerator design code ZAP [6].

In what follows, we first describe our experimental observations and interpretation of the linear properties of the Aladdin ring, including beta function and dispersion measurements. Next, we describe two experiments to measure the ring impedance, the first a measurement of the parasitic mode loss, and the second a measurement of the beam transfer function. Then, measurements of the longitudinal and transverse emittance at 100 and 200 MeV are described and compared with IBS predictions. Finally, we give a summary of our experimental findings and recommendations for future work.

II. Linear Lattice Measurements

In this Section we describe our measurements of the linear lattice parameters, the beta functions and dispersion. To give a feeling for the approach we have taken in our investigation, the story will be presented in a stepwise fashion, more or less in chronological order. A diagram of the Aladdin ring is presented in Fig. 2; the locations of the various magnets alluded to in the following discussion are indicated.

Beta Function Measurements

The technique used to measure the beta values was that of shunting the various quadrupoles and measuring the resultant tune shift. If the change in quadrupole current is ΔI_Q and the corresponding tune shift is Δv, then the beta value at that location is given by [7]:

$$\beta = \frac{4\pi\beta\rho}{K} \frac{\Delta v}{\Delta I_Q} [1 + \Delta v \cot (2\pi v)] \tag{1}$$

where $B\rho$ is the beam magnetic rigidity and K is tne constant that re-
lates the quadrupole current to its integrated gradient (in T/A). Because
the discrepancy with the model calculations was observed only in the verti-
cal plane, we will focus our interest on these results; the results from the
horizontal plane will be described briefly toward the end of this Section.

In carrying out our measurements, the nominal working point of the ma-
chine was moved away from the "acceleration" tunes of $v_{x,y} \simeq (7.1, 7.1)$
to (7.1,7.25), and ultimately to other values as well. This choice moves
away from the x-y coupling resonance and locates the vertical tune farther
from an integer tune value. Unless otherwise noted, the measurements were
carried out at 800 MeV.

In our first measurements of the vertical beta functions, it was found
that the maximum values we observed were significantly lower than those pre-
dicted by SYNCH based on the nominal magnet parameters. This is shown in
Fig. 3. The maximum predicted beta values, at the center quadrupole ("Q2")
of the quadrupole triplet at each end of the long straight section (see
Fig. 2), are about 20 m, whereas the observed beta values were only about
10-14 m. Although more or less equivalent discrepancies occur in other lo-
cations, the differences between theory and experiment were most clearly no-
ticeable at the Q2 locations. For this reason, we concentrated our efforts
on measurements of the beta functions at these particular locations.

Concentrating on just the Q2 locations, we see from Fig. 4 that the ob-
served pattern corresponds to a superperiodicity of N = 1, rather than the
expected fourfold symmetry or even the previously reported twofold symmetry.
Although there are significant changes in the observed pattern (see Fig. 4)
when the chromaticity sextupoles are turned off, the overall symmetry does
not change.

In order to understand these observations, W. Bliss of the SRC staff attempted to model the data with SYNCH; the results are shown in Fig. 5. Clearly the agreement with experiment is improved, although some discrepancies remain. The calculated results in Fig. 5 correspond to adjusting the relative strengths of the five quadrupole power supplies (QF, QD, Q1, Q2, Q3) by amounts on the order of 2%. This adjustment appears to be within the calibration uncertainty of the control system and does not, in itself, suggest a serious problem. Nevertheless, the absence of the predicted fourfold symmetry in the data led us to try additional measurements.

In the next series of tests, we investigated the effect of varying the vertical tune (while keeping the horizontal tune roughly fixed at a value of 7.1). The results, shown in Fig. 6, indicate that there is always a minimum beta value at the location of quadrupole 4Q2A, independent of the tune value. We infer from this that there may be a perturbation 180° away from this location, i.e., at 2Q2A.

It turns out that our previously measured orbit data had already indicated a possible problem in this area of the lattice. There appears to be an unexplained "kink" in the orbit in this region (and in no other part of the ring) when the beam is centered at the beam position monitor (BPM) at 2Q2A; this must be caused by an unexpected dipole field component. Unfortunately, because of the distance between adjacent BPMs, it is not possible to isolate the problem specifically to 2Q2A. Hypotheses that are consistent with our observations include: (a) a roll error in BM3 that gives the beam a vertical deflection; or (b) a misalignment in either of the adjacent quadrupoles 2Q1A or 2Q3A that produces an extra dipole field in this region. The latter possibility was investigated briefly by shunting, in turn, each of the two adjacent quadrupoles and looking for a change in the vertical orbit;

in each case no orbit change was observed. Possibly this is due to the much lower vertical beta values in the adjacent quadrupoles (a factor of 4 lower than 2Q2A), but this is not certain. The former possibility remains to be studied. It is worth mentioning, however, that the installation at our behest of an additional vertical steering magnet in the vicinity of 2Q2A did lead to an immediate improvement in the observed vertical closed orbit and to a reduction in the strong x-y coupling observed when the beam is being kicked during the injection process.

With these facts in mind, W. Bliss was again asked to try to model our results, concentrating specifically on the area of 2Q2A. Further simulations showed improved agreement with our results if the gradient in quadrupole 2Q2A was assumed to be about 1% higher than that of the other Q2 quadrupoles with which it is in series. This is demonstrated in Fig. 7. We note that this explanation has the advantage (compared with the earlier attempt to adjust the relative values of all quadrupoles) of correctly predicting the experimentally observed lack of symmetry in the vertical beta functions.

Because the predicted effect corresponds to having too high a gradient in 2Q2A, it is straightforward to test it experimentally. To do so, we simply added a fixed shunt to 2Q2A that would remove about 1% of the current from the magnet and then remeasured the beta values in the ring. In Fig. 8, we show the results of trying several different fixed shunt values for 2Q2A. To limit the heating of the temporary shunt, these measurements were carried out at a reduced beam energy of 400 MeV. (Earlier tests at various energies had already demonstrated that the observed behavior of the beta functions was reproducible at energies below 800 MeV.) It can be seen from Fig. 8 that a 1% shunt does have the effect of reducing the very large excursions

at some quadrupole locations, and appears to make the measured values more regular in their behavior. Adopting for now tne 1% shunt value, we remeasured all of the vertical beta values both with and without the fixed shunt. Again we conclude (see Fig. 9) that the violent excursions are lessened when the fixed shunt is utilized.

To investigate the effects of the fixed 2Q2A shunt on the superperiodicity of the ring, we next carried out some "kick" measurements. Vertical steering magnets located at homologous points in each quadrant were used to provide an equivalent strength kick and the resultant orbit change throughout the ring was measured with the BPM system. The results are displayed in Fig. 10, where we plot the response in each of the other three quadrants relative to that in quadrant 1. The improvement in the symmetry of the responses is clearly apparent when the 1% fixed shunt is utilized, and we conclude from this that the superperiodicity is essentially $N = 4$ when the fixed shunt is used. When the fixed shunt is not used, we see that, while quadrant 3 behaves similarly to quadrant 1, quadrants 2 and 4 do not. The pattern seen in quadrants 2 and 4 appears very similar, however, and this similarity is confirmed by looking at the difference between these two quadrants in Fig. 11. Thus, within the accuracy of this technique, we observe a superperiodicity of 4 with the fixed 1% shunt and a superperiodicity of roughly 2 without it.

Further modeling of our results with SYNCH after returning to LBL indicates that the effect of the single quadrupole error manifests itself differently at different tune values. These results are displayed in Fig. 12, which shows the trends observed in both the measured and predicted beta functions at the various Q2 locations for several different values of the vertical tune. For these calculations we adopted a value of 1.5% for the

2Q2A error, as this value seemed to give better (qualitative) agreement with the modulation in beta functions seen at the lower tune values. We see from Fig. 12 that the single quadrupole error manifests itself as very nearly a twofold symmetry at a vertical tune of 7.1, whereas the symmetry is essentially onefold at a tune of 7.45. At intermediate tune values, the symmetry is actually onefold, but the difference between onefold and twofold symmetry is clearly more difficult to observe.

Before leaving the subject of beta functions, we should comment on the implications of our results on the horizontal beta functions. As mentioned earlier, the horizontal results have always agreed well with SYNCH predictions. It is natural, then, to ask what happens if we assume a 1% gradient error in 2Q2A. The answer is given in Fig. 13, which shows the predicted and measured horizontal beta functions for an assumed 1% error in 2Q2A. Clearly the agreement in the horizontal plane is maintained, because the predicted changes in beta function due to the error in the vertically focusing 2Q2A are essentially negligible.

Thus, we believe that there is a gradient error in quadrupole 2Q2A that is responsible for the observed lack of vertical symmetry in the ring. It appears that the existence of this error is not in disagreement with any of the observations of which we are aware. On the other hand, we note that various checks of 2Q2A, e.g., resistance and inductance measurements, have not indicated any observable problem. It seems clear that accurate field measurements of this magnet (and others) are called for.

Dispersion Measurements

We turn now to our check on the dispersion function at Aladdin. To do this, we made measurements in which we shifted the RF frequency by a small

amount and observed the resultant orbit change with the BPM system. Unfortunately, the hardware available to us at Aladdin allowed a change of RF frequency of only 5 kHz (out of 50 MHz), which corresponds to a momentum change of only about 0.3%. In order to obtain meaningful results, our measured data were averaged at homologous points around the ring. The measured data are compared with SYNCH predictions in Table I; the agreement is excellent and indicates no problem in our understanding of this aspect of the Aladdin lattice.

III. Impedance Measurements

In this Section we describe our measurements of the Aladdin ring broadband impedance. Two different techniques were employed: observation of the parasitic mode loss via the change in synchronous phase as a function of beam intensity, and measurement of the beam transfer function by modulating the RF phase and observing the corresponding changes induced in the beam. These experiments are discussed in turn below.

Parasitic Mode Loss Measurement

The energy loss of a circulating beam into parasitic modes is a beam current dependent collective phenomenon. It is determined by the resistive longitudinal electromagnetic coupling impedance experienced by the beam due to its surroundings. Circulating beam bunches lose energy by inducing wall currents at frequencies that drive (and hence deliver power to) the resonant parasitic modes of the storage ring, including the walls and the RF cavities. The process is usually quantified [8] by the parasitic mode loss parameter, k. For a stable stored beam, the energy loss means that the synchronous phase angle of the bunch, ϕ_s, must increase with increasing bunch current in order to compensate for the increasing loss.

At Aladdin, we measured the parasitic mode loss parameter by measuring the relative phase between the 50 MHz signal from the RF cavity and from the beam (i.e., the filtered RF component of the bunch signal) as a function of beam intensity. The experimental setup is illustrated schematically in Fig. 14.

Experiments were carried out at a beam energy of 100 MeV using a single stored bunch with the 50 MHz RF system. The observed shift in synchronous phase angle as a function of beam intensity is shown in Fig. 15. From these data we extract a value for the slope of

$$\frac{d(\Delta\phi_s)}{dI} = 0.61°/mA \quad .$$

For a peak RF voltage of V_{RF} = 1.8 kV, this slope corresponds to a parasitic mode energy loss per unit of beam current of

$$\frac{dU_{pm}}{dI} = V_{RF} \cos \phi_s \frac{d(\Delta\phi_s)}{dI} \simeq 19 \text{ eV/mA} \tag{2}$$

(assuming negligible energy loss due to synchrotron radiation at this low energy). The experimental value of the parasitic mode loss parameter is then

$$k = k_B f_o \frac{dU_{pm}}{dI} = 6.5 \times 10^{10} \text{ V/Coul} \tag{3}$$

where k_B is the number of bunches (here k_B = 1), and f_o is the bunch revolution frequency (here f_o = 3.37 MHz).

To estimate the broadband impedance of the ring, we have modeled it by a broadband resonator with shunt impedance R_s, resonant frequency ω_R, and quality factor Q, whose (complex) impedance is given by

$$Z(\omega) = \frac{R_s}{1 - iQ\left(\frac{\omega_R}{\omega} - \frac{\omega}{\omega_R}\right)} \tag{4}$$

We chose the resonator to have Q = 1 and to be centered at a resonant frequency corresponding to the cutoff frequency of the beam pipe. For Aladdin, the effective radius of the vacuum chamber is about 3 cm, which implies a cutoff frequency of $\omega_R \approx 10$ GHz ($f_R \approx 1.7$ GHz).

The parasitic mode loss parameter can be expressed as an integral over frequency of the product of the impedance and the frequency spectrum of the bunch. For a Gaussian bunch with rms length σ_ℓ, k is given by [9]:

$$k = \frac{1}{2\pi} \int_{-\infty}^{\infty} Z(\omega) \exp(-\omega^2 \sigma_\ell^2/c^2) d\omega \quad . \tag{5}$$

In the case where ($\omega_R \sigma /c$) >> 1, the integral becomes approximately

$$k \simeq \frac{R_s \omega_R}{4\sqrt{\pi}} \left(\frac{c}{\omega_R \sigma_\ell}\right)^3 \quad . \tag{6}$$

For the range of beam intensities used in our experiment (1-10 mA), the average rms bunch length is taken to be 15 cm. This value is consistent with the intrabeam-scattering-dominated bunch length predicted by ZAP [3]; it is also consistent with the full bunch length derived from a measurement of the dipole mode transfer function, to be described below. Because ($\omega_R \sigma_\ell/c$) $\approx$ 6 in our case, we can safely use Eq. (6) to analyze our results. We find that the shunt impedance of the equivalent Q = 1 resonator, Eq. (4), consistent with the observed parasitic mode loss parameter is R_s = 6.6 kΩ. The corresponding value for $\left|Z/n\right|_0$, the absolute value of the impedance Z divided by the mode number n = (ω/ω_0), is then

$$\left|\frac{Z}{n}\right|_0 = \frac{R_s}{(\omega_R/\omega_0)} \approx 13\,\Omega \quad . \tag{7}$$

The experimentally determined broadband impedance of Aladdin is thus represented by the model for the real part illustrated in Fig. 16.

Because the impedance value derived from a measurement of the parasitic mode loss is extremely sensitive to the bunch length, as follows from Eq. (6), precise knowledge of the bunch length is of paramount importance. In this sense, the previously reported value [4] of $\left|Z/n\right|_0 = 17\,\Omega$ is not in contradiction with our value of $1^?$ In view of the extreme sensitivity to bunch length, we have also attempted to measure the bunch length directly from the signal induced on a longitudinal beam pickup; the technique will be described below in Section IV. Although there are experimental difficulties in such measurements for the bunch length regime of interest here, the results were again consistent, within experimental errors, with the value adopted for our analysis.

Beam Transfer Function Measurement

The parasitic mode loss experiment just described provides us with an estimate of the resistive part of the longitudinal broadband impedance of the Aladdin ring. It is also of interest to investigate the reactive part of the impedance, which leads to a shift of the coherent synchrotron frequency as a function of beam intensity. This effect will manifest itself in the longitudinal beam transfer function, measured over a range of frequencies, for a given longitudinal mode. The effect is strong for the longitudinal quadrupole synchrotron mode, but is usually weak for the dipole mode.

Unfortunately, we were unable to perform the more sensitive quadrupole mode transfer function measurement due to the limited bandwidth available for amplitude modulation of the RF at twice the synchrotron frequency. We therefore measured the longitudinal dipole mode response of the beam

bunches. The dipole mode was excited by phase modulating the RF voltage at and around the synchrotron frequency. (The phase modulation was actually achieved by frequency modulating the master oscillator that drives the RF cavity.) The complex signals from the cavity loop (which measures the RF voltage seen by the beam) and from a longitudinal pickup located downstream (which gives the current modulation imposed on the beam) are compared through a network analyzer, and the resulting amplitude and phase transfer at the frequency of the modulation are obtained directly.

The longitudinal dipole mode transfer function was measured at 800 MeV for two different average bunch intensities (4.8 and 13 mA) in the multi-bunch mode with all 15 RF buckets occupied. Figures 17 and 18 show the resulting phase and amplitude response over a frequency range of 4 to 7 kHz, which spans the first dipole synchrotron band. A residual (and unexplained) phase shift, linear with frequency, is clearly visible as a slope in the phase response at frequencies well outside of the dipole band. This has been corrected for in the analysis by subtracting the slope from the observed response, as shown by the dashed lines in Figs. 17 and 18. The corrected phase response has the physically expected features of constant phase far outside the band of incoherent synchrotron frequencies occupied by the beam and a phase jump of 180° across the band. The maximum of the amplitude response curve corresponds to the coherent dipole mode frequency of the bunch, while the frequency width over which the 180° phase jump occurs is a measure of the incoherent synchrotron frequency spread in the bunch.

The coherent dipole mode frequencies obtained from Figs. 17 and 18 are 6 kHz (at 4.8 mA) and 6.2 kHz (at 13 mA), respectively. These values are plotted as a function of beam intensity in Fig. 19. Ideally, the intercept of this line (corresponding to the coherent dipole mode frequency in the

limit of zero current) provides a measure of the incoherent synchrotron frequency at the bunch center; the data in Fig. 19 give a value of 5.88 kHz. With only two measured points, of course, this value is only an estimate. The incoherent synchrotron frequency spreads in the bunches can be obtained from the phase curves in Figs. 17 and 18; they are $\Delta f_s \simeq$ 0.5 kHz at 4.8 mA and $\Delta f_s \simeq 1$ kHz at 13 mA. Assuming that the bunches occupy only a small fraction of the bucket, and that the bucket is otherwise unaffected by potential-well distortion effects, the nonlinear synchrotron frequency as a function of synchrotron amplitude can be taken to be of the octupolar type:

$$f_s(a) = f_s(0) \left(1 - \frac{h^2 a^2}{16} \right) \tag{8}$$

where h (=15 here) is the RF harmonic number and a is the amplitude of synchrotron oscillation (measured in units of angle around the ring). The bunch length (also measured in units of angle around the ring) is then given in terms of the full spread in synchrotron frequency by

$$\Delta \theta = 2a_{max} = \frac{8}{h} \left(\frac{\Delta f_s}{f_s(0)} \right)^{1/2} . \tag{9}$$

Values for the full bunch length derived in this manner are $\Delta t_{bunch} \simeq$ 6 ns at 4.8 mA and 8.5 ns at 13 mA.

Plots of the inverse of the complex beam response in the complex plane ("stability diagrams") are shown in Fig. 20 for both the 4.8 mA and 13 mA cases. These stability diagrams are shifted from their location in the absence of an impedance by a vector proportional to the actual impedance. Because the position of the unshifted stability diagram is, in general, unknown, the impedance can only be obtained from measurements carried out with

14

at least two different beam intensities. Given our determination of the re-
sistive part of the impedance (from the parasitic mode loss experiment de-
scribed above), the reactive part can be obtained from the slope of the
coherent frequency shift vs. beam current, which we find from Fig. 19 to be

$$\frac{df_s}{dI} = 0.024 \text{ kHz/mA} \quad .$$

The coherent frequency shift for the coupled-bunch longitudinal dipole mode
is given by [10]:

$$\Delta f_s = \frac{f_s}{2} \frac{I}{3B_0^3 \, hk_B V_{RF} \, \cos \phi_s} \left(\frac{Z_{\parallel},n}{n}\right)_{\text{eff., reactive}} \quad (10)$$

where B_o is the bunching factor, f_s is the synchrotron frequency, and
the other symbols have been defined earlier. The observed slope of
0.024 kHz/mA corresponds to a reactive part of the Aladdin ring impedance of
about 12 Ω.

We should point out here that there was evidence of substantial cou-
pled-bunch dipole oscillations at 800 MeV during our beam transfer function
measurements. This is evidenced in Fig. 21, which shows the spectrum around
the second harmonic of the RF frequency (with no phase drive) at 800 MeV and
a beam intensity of 6.1 mA. Two synchrotron dipole oscillation sidebands
are observed (with significant strength), on both sides of the betatron
band, spaced by about 6 kHz (the synchrotron frequency) from the central
line. Consequently, our beam transfer function measurements might have been
affected by these spontaneous dipole motions. Fortunately, the phase re-
sponse, which contains most of the information, is not expected to be se-
riously affected by these background oscillations.

IV. **Emittance Measurements**

At low energies (say 100 MeV), our calculations [3] on Aladdin lattices predicted large transverse and longitudinal emittance growth. This is shown in Figs. 22 (transverse) and 23 (longitudinal), which are reproduced from Ref. [3]. The natural horizontal emittance at 100 MeV is 1×10^{-9} m-rad, so the indicated equilibrium emittance values correspond, in the worst case, to an increase of almost a factor of 1000. (For the representative case of 10:1 emittance coupling and 100 mA of beam current, the growth is a factor of 400.) Similarly, at a beam current of 100 mA the bunch length and momentum spread increase by a factor of about 16 compared with their natural values. (It should be noted that this longitudinal growth occurs even for a beam that has already blown up longitudinally to the limit imposed by the microwave instability.)

Insofar as there is often interest in building electron storage rings with relatively low energy injectors, it was felt to be very worthwhile to investigate at Aladdin whether the predicted large emittance growth occurs and, if so, whether its beam intensity dependence is as expected from IBS considerations.

To obtain the transverse emittance, we measured the transverse beam size using the emitted synchrotron radiation. The light from the upstream port of dipole BM2 is focused onto two silicon diode arrays coupled to a scanning system that produces a profile from which the rms beam widths can be obtained.

The longitudinal measurements were made via a longitudinal pickup that is capacitively coupled to the beam. Unfortunately, the pickup was limited in bandwidth, and this was exacerbated by a lack of suitable cabling to connect the system to the fast oscilloscope in the control room.

To avoid measurement problems associated with the severe longitudinal coupled-bunch oscillations seen in Aladdin at low energies, it is desirable to perform the experiment with only a single bunch circulating in the ring. However, the present inability at Aladdin to inject and accelerate a large amount of current in a single bunch would have limited our ability to obtain information about the intensity dependence of the emittance.

For both of the above reasons, it was decided to consider utilizing the first-harmonic (3.37 MHz) RF cavity that was available. With this choice, the bunch length would be much greater than for the fifteenth harmonic cavity, and consequently the measurement would be much less susceptible to the cabling limitations alluded to above. Moreover, the amount of current that could be accelerated in a single bunch is higher than for the h = 15 system, so this parameter would be easier to vary. The drawbacks of such a choice are that the larger beam size diminishes the effect of the IBS (all other things being equal) and that the energy range available with the h = 1 RF system is limited to below about 200 MeV. Because the former drawback is roughly compensated by the increase in available beam intensity, and the latter is not a concern because of the rapid decrease in IBS with increasing beam energy [3], we chose to use the first-harmonic cavity. A typical bunch length profile is shown is Fig. 24.

For the momentum spread, no direct experimental measurements were made. Therefore, it was necessary to infer this parameter from the measured bunch length and the known RF parameters:

$$\sigma_p = \frac{v_s \sigma_\ell}{\eta R} \tag{11}$$

where v_s is the synchrotron tune, η is the frequency slip factor, and R is the average ring radius.

As it turns out, the momentum spread is also very important in the determination of the horizontal emittance, because the transverse emittance is measured at a location in the ring where the dispersion is nonzero. The horizontal emittance is obtained from the measured beam size by:

$$\epsilon_x = \frac{\sigma_x^2 - D^2 \sigma_p^2}{\beta_x}$$ (12)

where σ_x is the rms horizontal beam size, D is the dispersion at the measurement location, β_x is the horizontal beta function, and σ_p is the rms relative momentum spread.

The vertical emittance does not depend on the momentum spread, since we assume zero dispersion in this plane, and is given by:

$$\epsilon_y = \frac{\sigma_y^2}{\beta_y} .$$ (13)

The results of our measurements, along with predictions from ZAP, are given in Table II for both 100 and 200 MeV. It is clear that there is considerable transverse emittance growth (about a factor of 200) compared with the natural emittance at 100 MeV, whereas at 200 MeV the growth is much smaller (about a factor of 10). Although the trends predicted by ZAP are qualitatively similar, the transverse emittance is underpredicted by about a factor of 2. It is probable that at least some of this discrepancy is due to emittance blowup from interactions with the residual gas and with trapped ions. In any case, the extreme blowup we predicted [3] is clearly present and is even worse than expected.

With regard to the longitudinal growth, it is found that the magnitude of the bunch length is somewhat overpredicted at 100 MeV but is given quite accurately at 200 MeV. At both energies, however, the trend of bunch length

vs. current agrees more closely with the IBS predictions than with the behavior expected from the longitudinal microwave instability. For example, at 100 MeV the intensity range covers a factor of 14, which leads to a predicted decrease in bunch length by a factor of 2.5 if the dominant effect were turbulent bunch lengthening. On the other hand, the IBS calculations predict a decrease of only 38%. The observed decrease of 25% clearly supports the latter model. A similar statement applies at 200 MeV.

Based on the present investigation, it seems clear that the importance of the intrabeam scattering process to the emittance of a low energy electron storage ring has been verified. The observed longitudinal and transverse emittances can be several orders of magnitude larger than the natural values, and this must be taken into account in the design of a low energy injection system.

V. Summary

We have reported here on a series of experimental measurements of the Aladdin storage ring that were carried out during the latter part of April, 1985. Linear lattice properties (beta functions, dispersion) have been measured and, for the horizontal plane, were found to agree well with predictions of the lattice code SYNCH. In the vertical plane, the observed discrepancies with the model calculations have been traced to a gradient error (of about 1%) in a particular vertically focusing quadrupole, 2Q2A. Model calculations assuming such an error have been found to give much improved agreement with measured beta functions, and experiments in which the offending quadrupole is shunted by about 1% lead to more regular behavior of the vertical beta functions throughout the ring and restore the expected four-fold symmetry in the vertical plane. Although the error found in 2Q2A seems

clearly to be larger than those of the other ring magnets, it is still our strong recommendation that all of the Aladdin magnets be carefully measured.

Measurements of both the resistive and reactive components of the storage ring broadband impedance have also been made, leading to values of 13Ω and $12\,\Omega$, respectively. These values are in reasonable agreement with earlier estimates and a previous experimental study.

Finally, measurements have been made of the longitudinal and transverse emittance at beam energies of 100 and 200 MeV. The observed values show substantial growth from the natural emittance and are roughly consistent with calculations of the emittance blowup expected from intrabeam scattering. We conclude from this that the intrabeam scattering process can strongly influence the performance of a low energy electron storage ring, and should be taken into account in the design of a low energy injection system.

In terms of future experiments, we believe that the main goal should be to understand and eliminate the severe x-y coupling observed in the machine. In addition, vigorous pursuit of the severe ion trapping problems seen in the ring must clearly continue.

Acknowledgments

Table I

Dispersion Data

	Position	Dispersion (m) SYNCH	Measured
Arc	QF1	0.65	0.61 ± 0.16
	QF2	1.40	1.38 ± 0.14
	QF3	1.36	1.39 ± 0.14
Straight	Q1A	0.64	0.64 ± 0.11
	Q3B	−0.94	−1.03 ± 0.15

Table II

Emittance Data

100 MeV

I (mA)	$\varepsilon_x^{meas.}$ [a] (10^{-8} m-rad)	ε_x^{ZAP} [b] (10^{-8} m-rad)	$\varepsilon_y^{meas.}$ (10^{-8} m-rad)	$\sigma_\ell^{meas.}$ (m)	σ_ℓ^{ZAP} [b] (m)	$\sigma_\ell^{\mu wave}$ [b] (m)
7.6	23.7 ± 7.3	11.2	15.7	1.0	1.5	1.0
4.9	23.7 ± 7.3	12.1	9.5	1.0	1.4	0.84
1.1	10.6 ± 3.9	6.9	4.8	0.84	1.1	0.51
0.52	6.6 ± 2.8	4.5	<4.5	0.75	0.93	0.40

200 MeV

I (mA)	$\varepsilon_x^{meas.}$ [a] (10^{-8} m-rad)	ε_x^{ZAP} [b] (10^{-8} m-rad)	$\varepsilon_y^{meas.}$ (10^{-8} m-rad)	$\sigma_\ell^{meas.}$ (m)	σ_ℓ^{ZAP} [b] (m)	$\sigma_\ell^{\mu wave}$ [b] (m)
4.0	4.4 ± 2.5	2.9	1.3	1.1	0.96	0.79
2.0	4.6 ± 2.4	2.5	1.1	1.1	0.88	0.63
1.0	4.3 ± 1.9	2.0	0.94	0.9	0.80	0.50
0.5	4.4 ± 1.6	1.8	0.78	0.78	0.73	0.41

[a] Assumed errors are: $\sigma_{x,y}$, 10%; $\beta_{x,y}$, 10%; D, 10%; σ_ℓ, σ_p, 20%.

[b] Based on a broadband impedance of 13 Ω.

References

[1] S. Chattopadhyay, "Coherent Instability and Ion Trapping Considerations for Aladdin Lattices," Lawrence Berkeley Laboratory Report No. LBL-19281, (May, 1985).

[2] A. Jackson, "The Dynamic Aperture of Aladdin," Lawrence Berkeley Laboratory Report No. LBL-19350,(March, 1985).

[3] M. S. Zisman, "Parametric Studies of Aladdin Lattices," Lawrence Berkeley Laboratory Report No. LBL-19191,(March, 1985).

[4] A. Hofmann and P. Morton, SLAC, (private communication).

[5] H. Lancaster and J. Bisognano, "Estimate of SRC Broadband Coupling Impedance," LBL Engineering Note, January, 1985 (unpublished).

[6] Code ZAP, J. Bisognano, S. Chattopadhyay, and M. S. Zisman, Lawrence Berkeley Laboratory, (unpublished).

[7] J. Borer, A. Hofmann, J-P. Koutchouk, T. Risselada, and B. Zotter, IEEE Trans. Nucl. Sci., NS-30, 2406(1983).

[8] A. Hofmann and T. Risselada, IEEE Trans. Nucl. Sci., NS-30, 2400 (1983).

[9] P. Wilson, J. Styles, and K. Bane, IEEE Trans. Nucl. Sci., NS-24, 1496 (1977).

[10] J. L. Laclare, "Bunched Beam Instabilities," Proc. of Intl. Conf. on Part. Accel., Geneva, July, 1980.
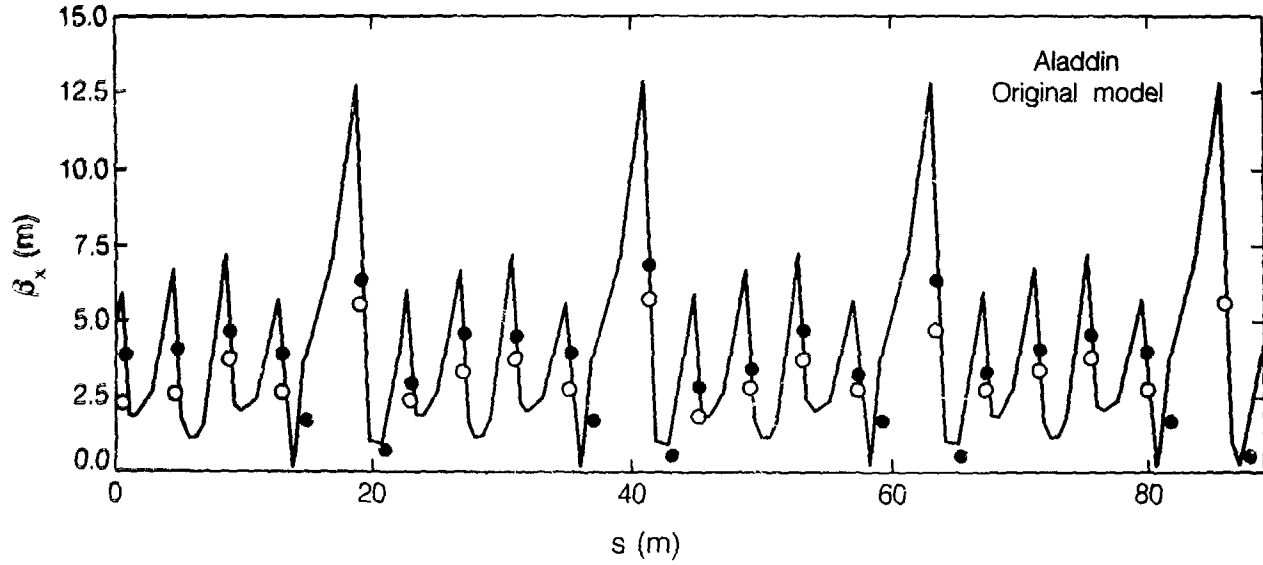
XBL 857-3074

Fig. 1   Comparison of measured (points) and predicted (solid curve) horizontal
         beta functions based on the original model of the Aladdin lattice.

Inverse compton
scattered beamline

Normal
synchrotron
radiation ports

40 mr port
(TYP.)

50 mr port
(TYP.)

60 mr port
(TYP.)

2Q1A   2Q3B   2Q1B
QF3   QD3   2Q3A
QD2
BM3   2Q2A   2Q2B   QF5
BM2   QD5
⑦   BM5
QF2
QD1   BM1
QF1
1Q2B
⑥   ⑧
⑤
1Q2A
④
③
BM11
②   4Q2B   4Q2A
①
3Q2A
3Q2B
BM8

1. Focusing quadrupole   5. Accelerating cavity
2. Defocusing quadrupole   6. Vert. extraction magnet
3. Sextupole corrections   7. Injection kicker magnet
4. Extraction kicker   8. 100 MeV microtron

ALADDIN
1 GeV
Electron storage ring   0 1 2 3 4 5
                              Meters
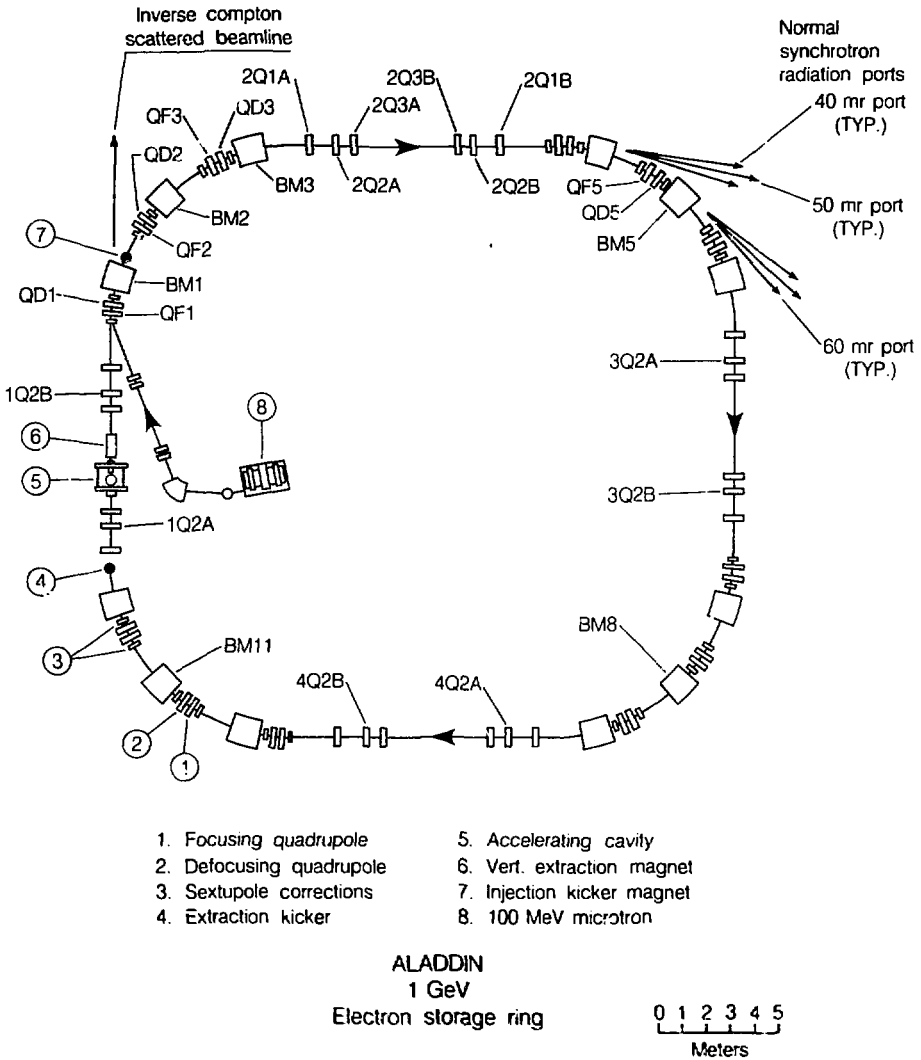
XBL 857-3067

Fig. 2   Diagram of the Aladdin storage ring. Magnet locations
         are indicated.
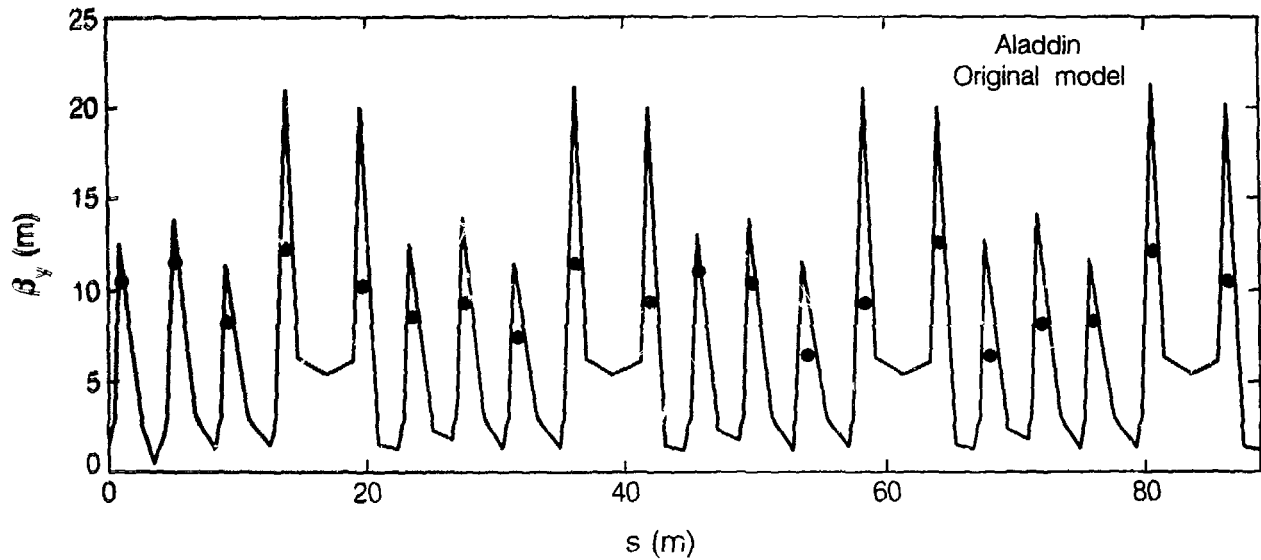
24

Fig. 3   Comparison of measured (points) and predicted (solid curve) vertical beta
         functions based on the original model of the Aladdin lattice.

Sextupoles off

$\nu_y = 7.23^*$

β_y (m)

Quadrupole position

Sextupoles on

$\nu_y = 7.29^*$

β_y (m)

Quadrupole position
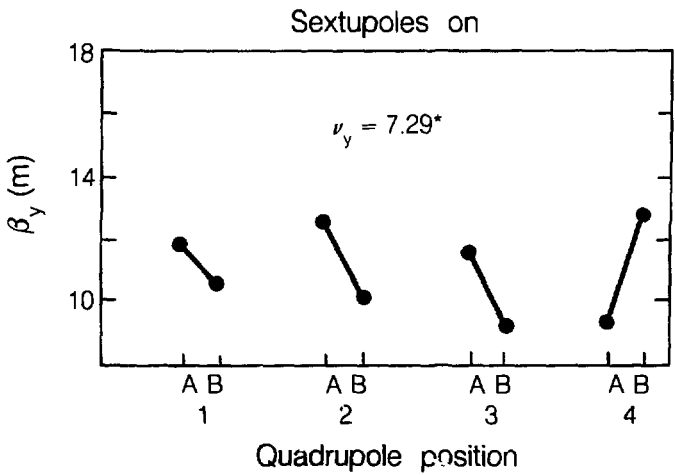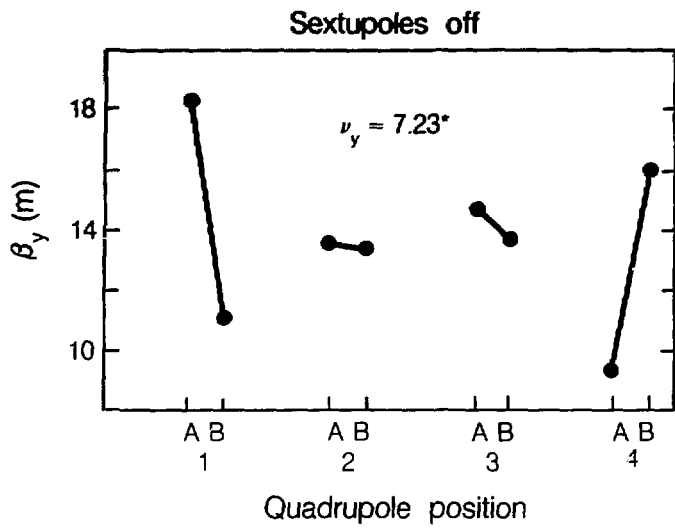
$^*\nu_x \sim 7.1$

XBL 857-3068

Fig. 4 Observed vertical beta function patterns at the loca-
tions of the Q2 quadrupoles, both with and without the
chromaticity sextupoles.
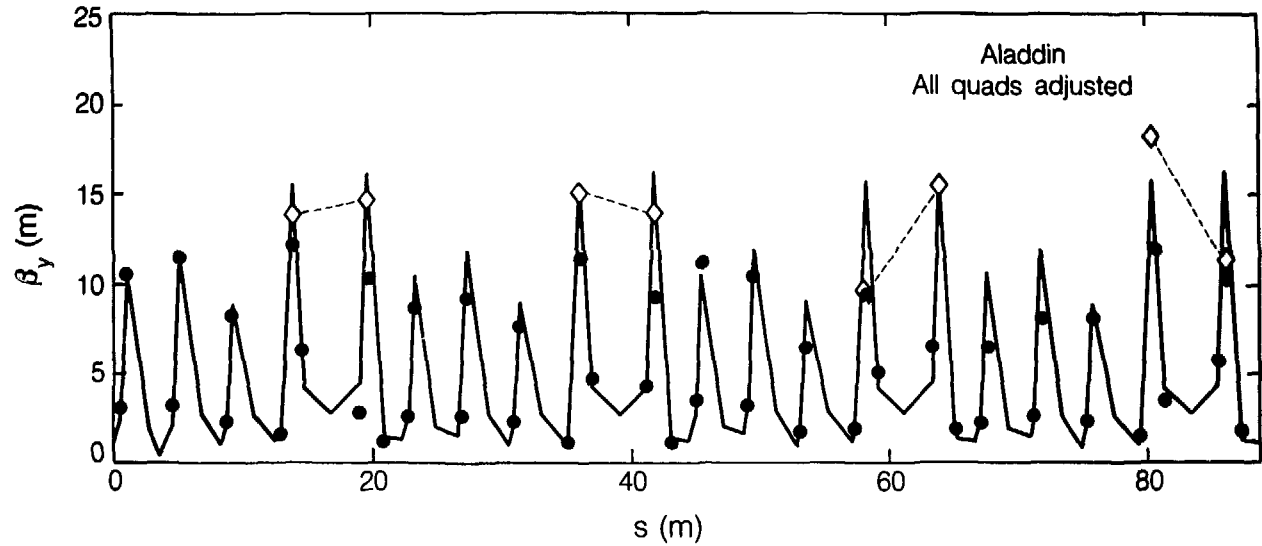
XBL 857-3077

Fig. 5   Comparison of measured (points) and predicted (solid curve) vertical beta functions based on a modified version of the Aladdin lattice. Measurements without the chromaticity sextupoles are indicated by diamonds.
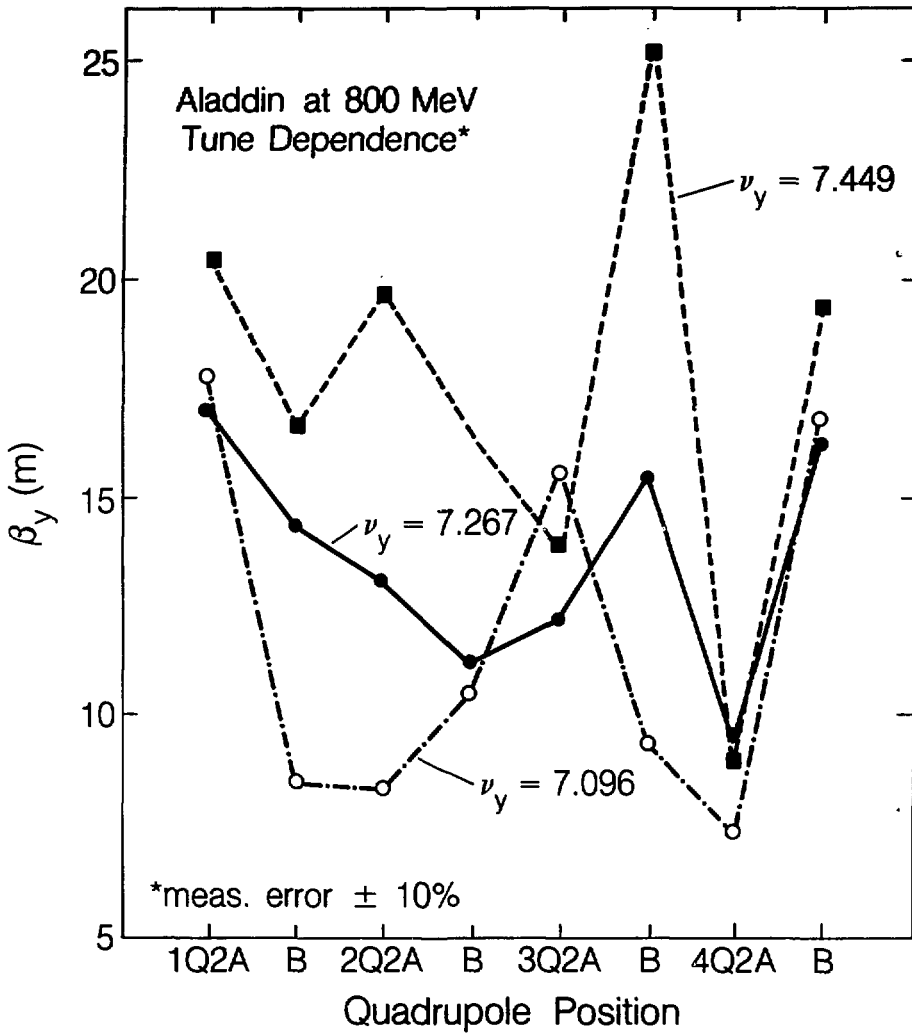
Fig. 6   Observed tune dependence of vertical beta functions at
the locations of the Q2 quadrupoles.
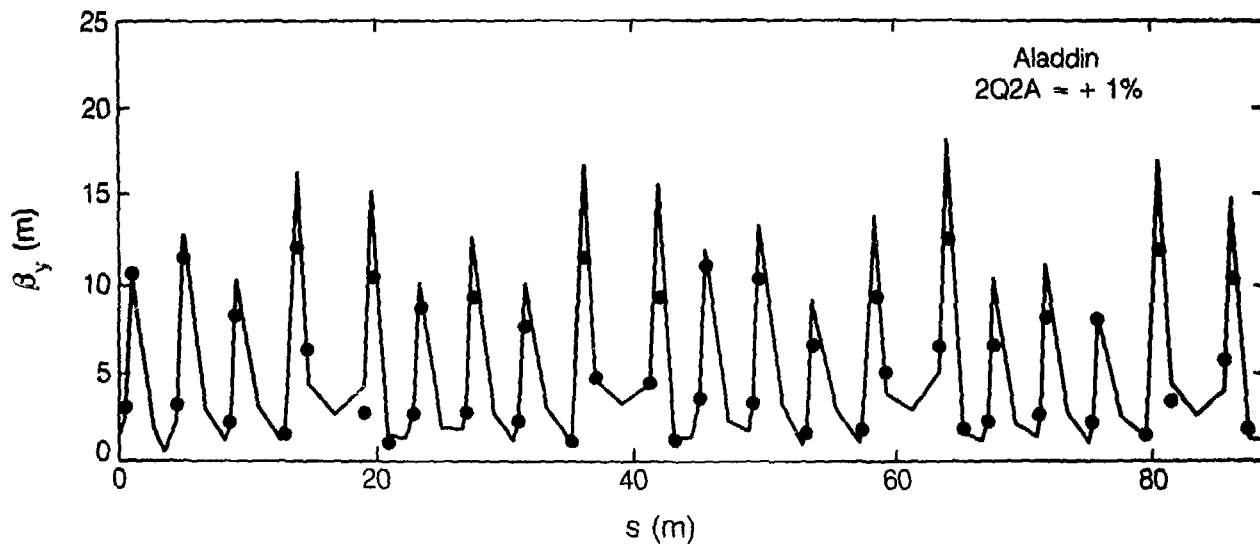
XBL 857-3076

Fig. 7   Comparison of measured (points) and predicted (solid curve) vertical beta functions under the assumption that quadrupole 2Q2A has an excess gradient of 1%.
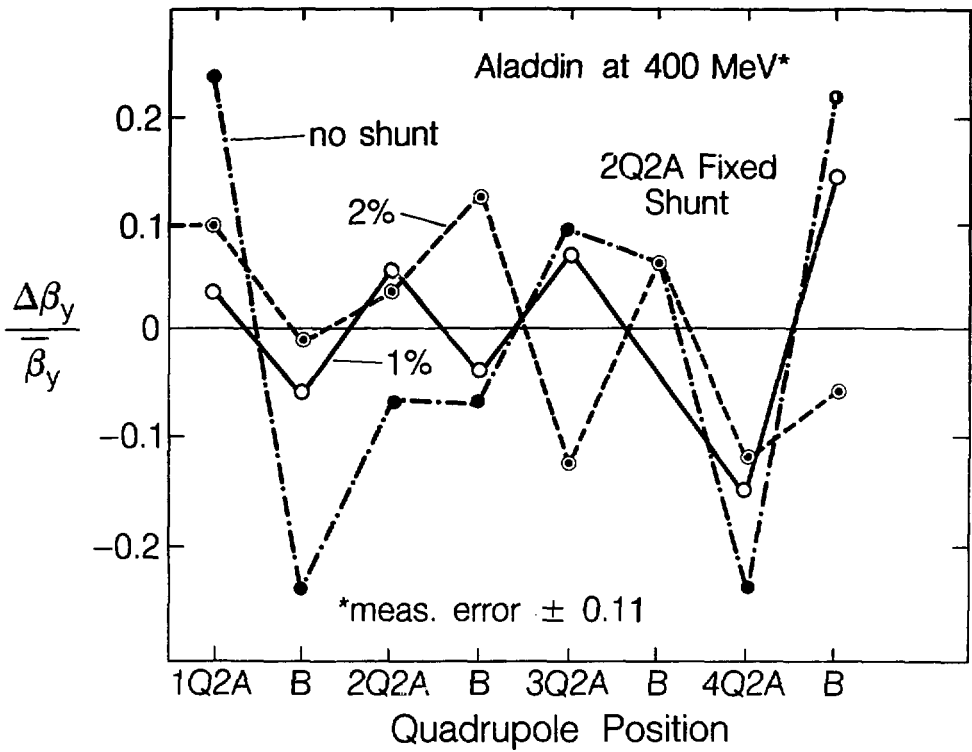
Fig. 8   Observed patterns of vertical beta functions for various fixed shunt values at quadrupole 2Q2A.
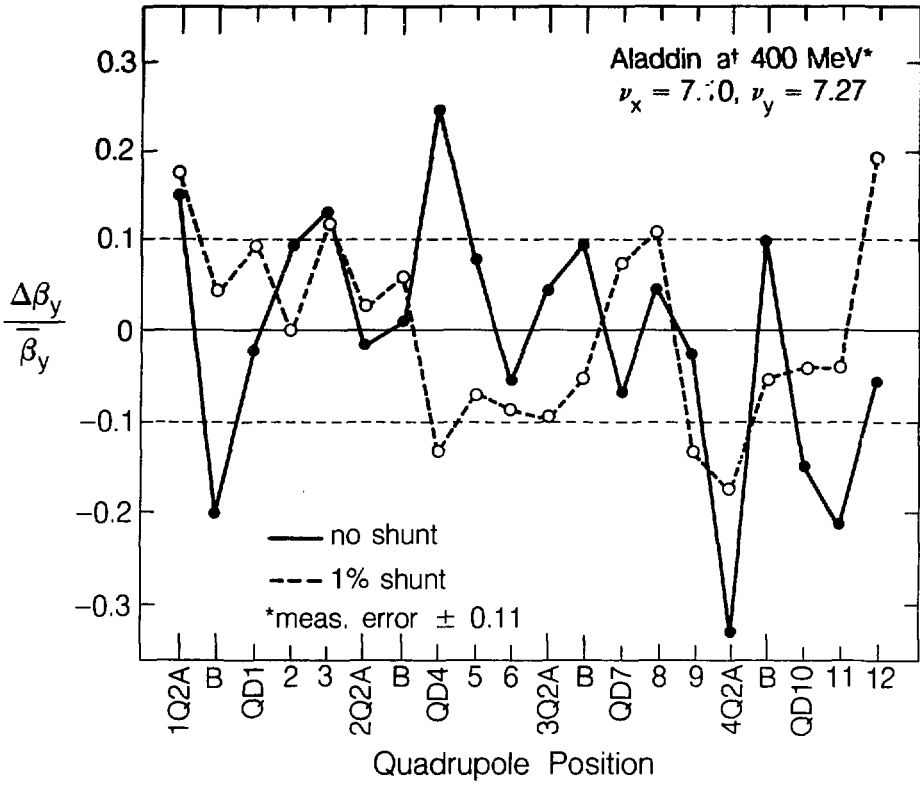
Fig. 9   Measured patterns of vertical beta functions both with
and without a 1% fixed shunt on quadrupole 2Q2A.
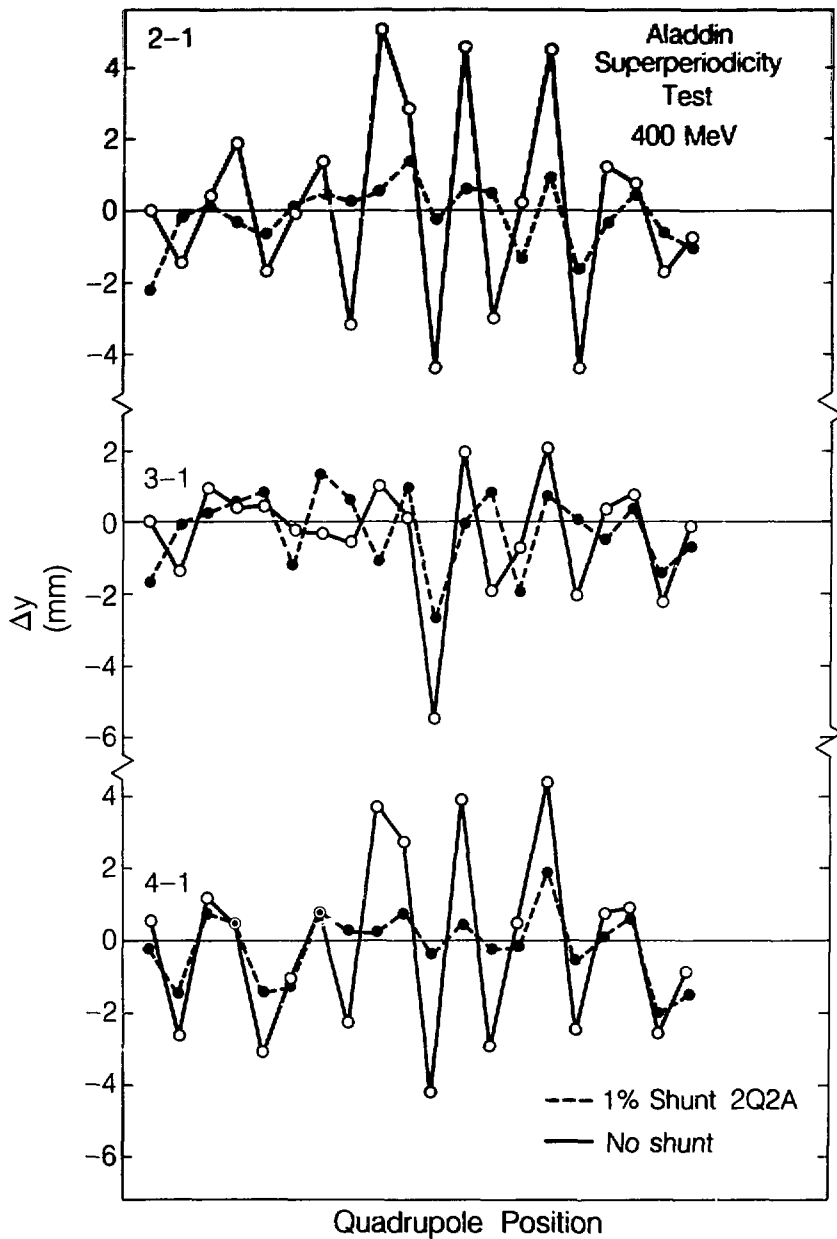
Fig. 10   Results of vertical kick measurements, plotted as
          differences between the orbit change observed in
          quadrant "n" and that in quadrant 1. Measurements
          both with and without a 1% fixed shunt at quadrupole
          2Q2A are shown.
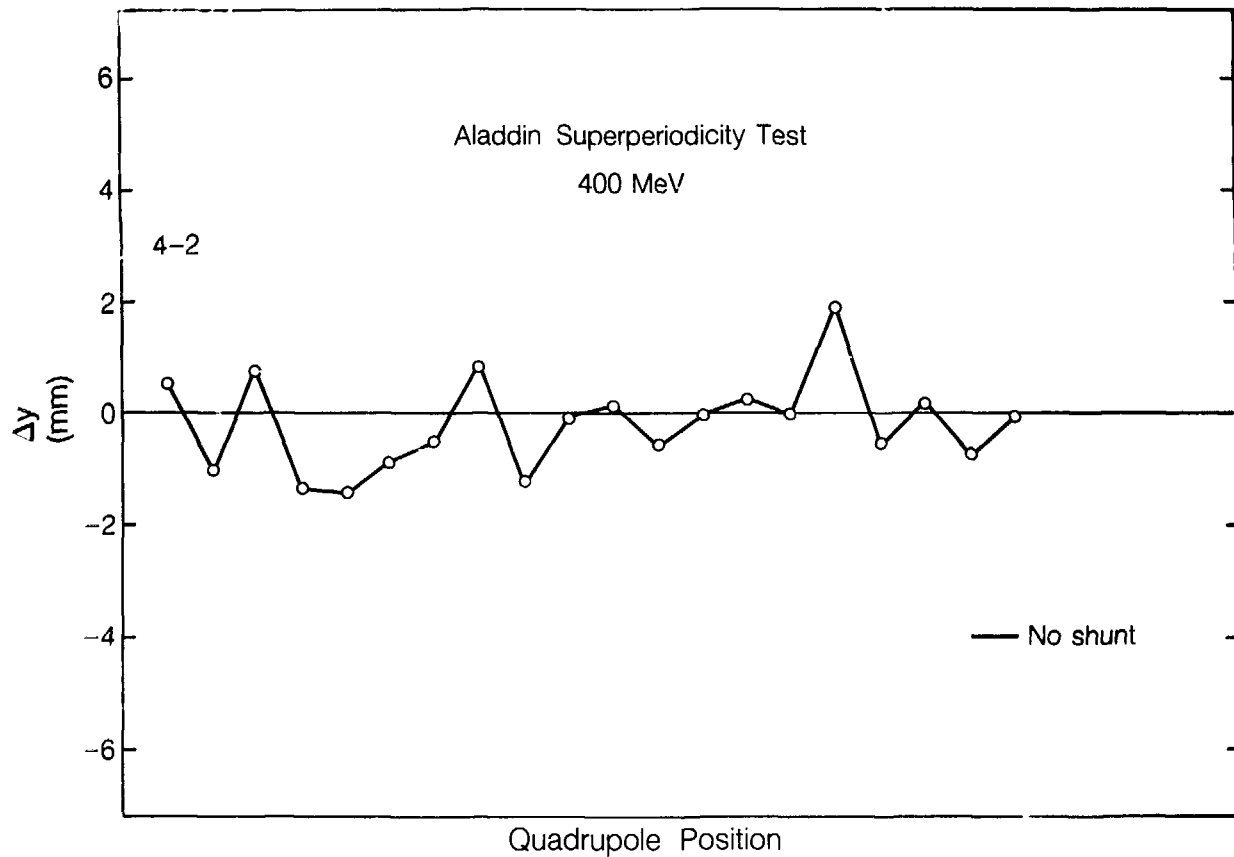
Fig. 11 Results of vertical kick measurements, plotted as differences between the orbit change in quadrants 4 and 2, for the case of no fixed shunt on quadrupole 2Q2A.

Fig. 12 Observed patterns of vertical beta functions at the
locations of the Q2 quadrupoles, for various values of
the vertical tune, compared with SYNCH predictions
assuming an excess gradient of 1.5% in quadrupole 2Q2A.
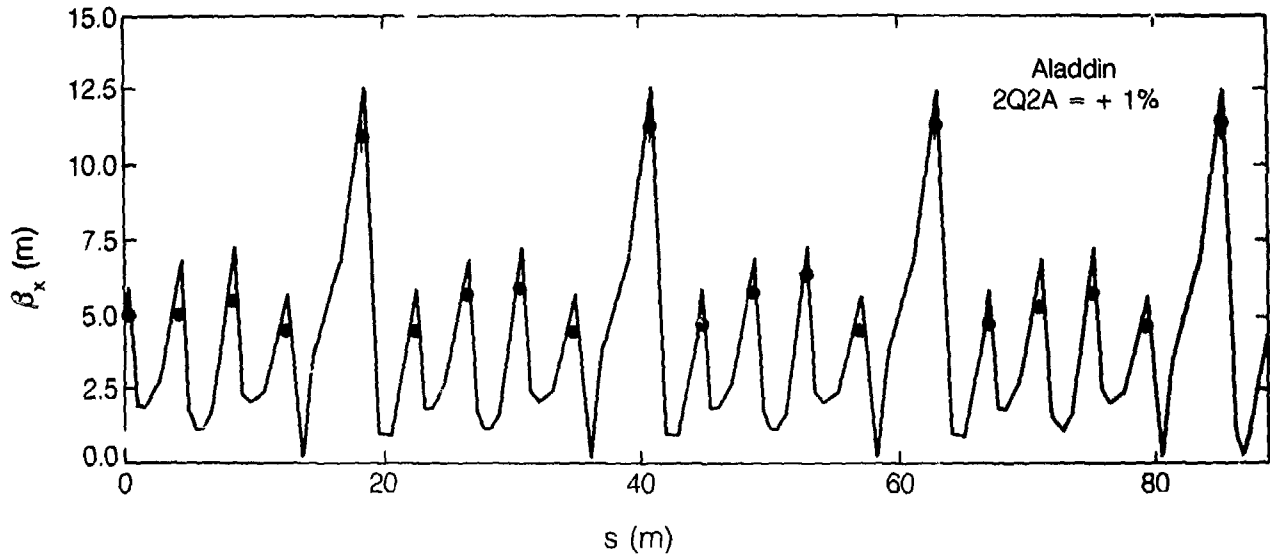
XBL 857-3072

XBL 857-3079

Fig. 13 Comparison of measured (points) and predicted (solid curve) horizontal
beta functions assuming an excess gradient of 1% in quadrupole 2Q2A.

RF Signal

Network
Analyzer

Cavity

Bunch

Pickup
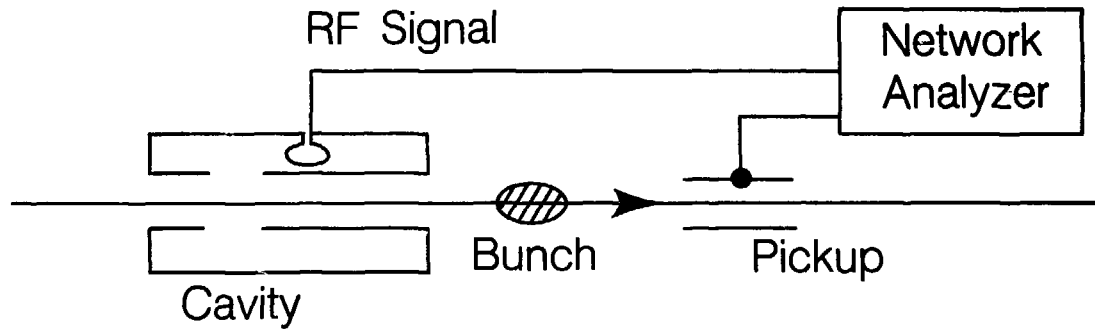
XBL 857-3066

Fig. 14 Schematic diagram of the parasitic mode loss experimental setup.
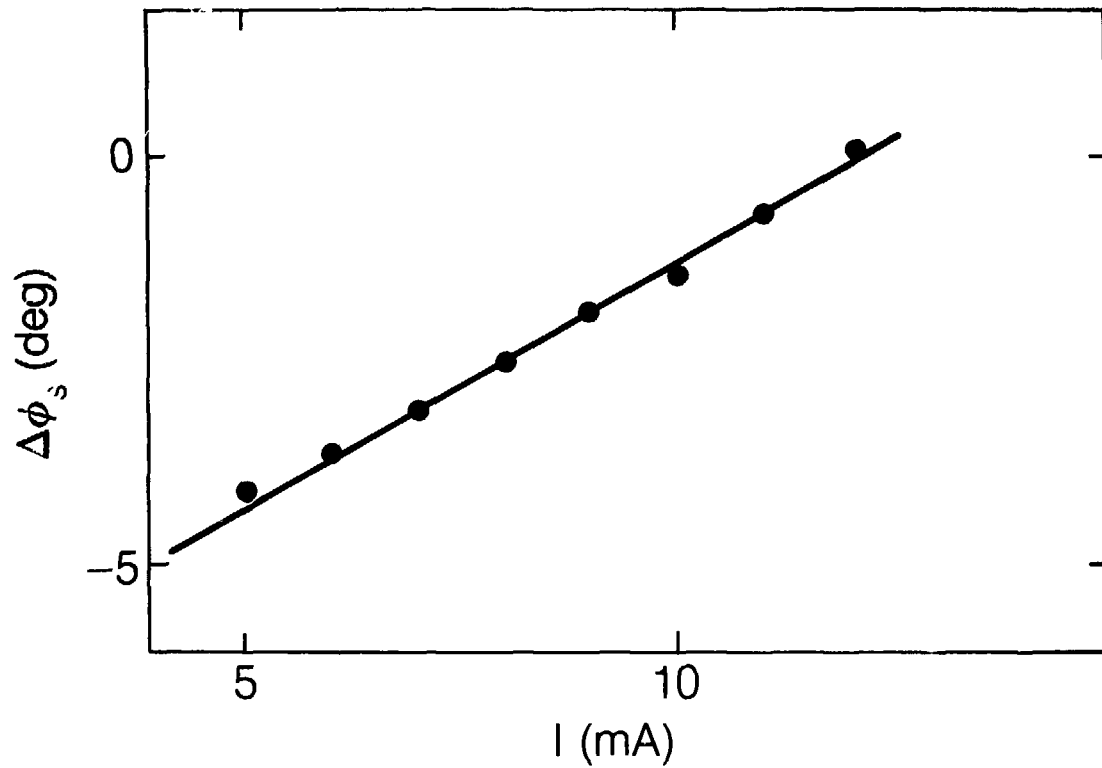
Fig. 15 Observed shift in synchronous phase angle as a function of beam intensity.
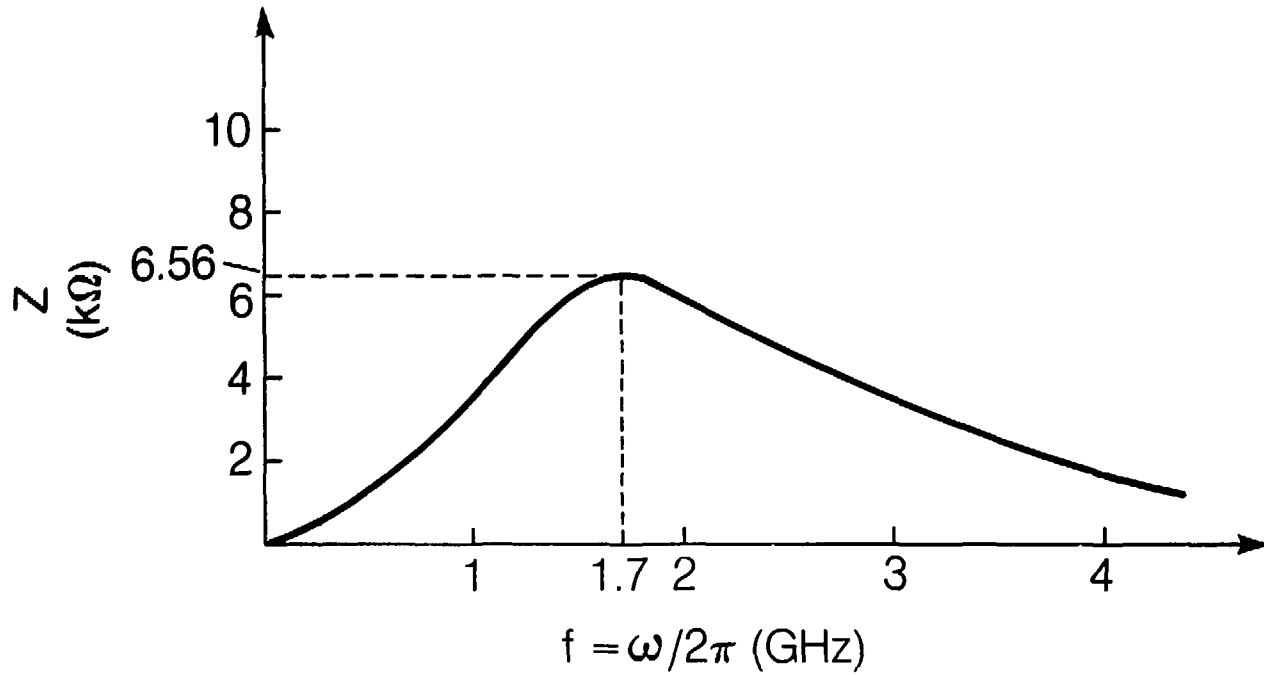
XBL 857-3063

Fig. 16 Model of the real part of the Aladdin broadband impedance.
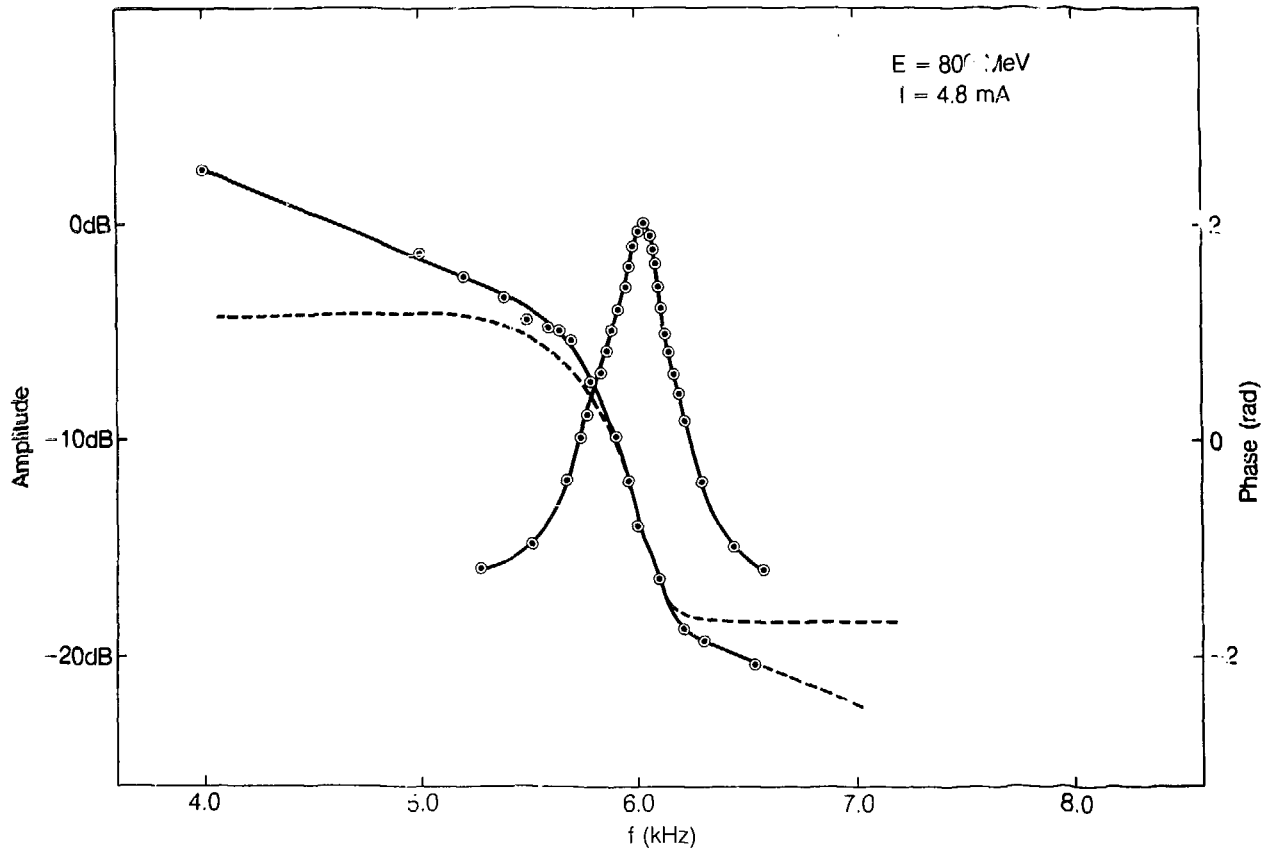
Fig. 17   Phase and amplitude response from the longitudinal dipole mode transfer
          function measurement at a beam intensity of 4.8 mA.
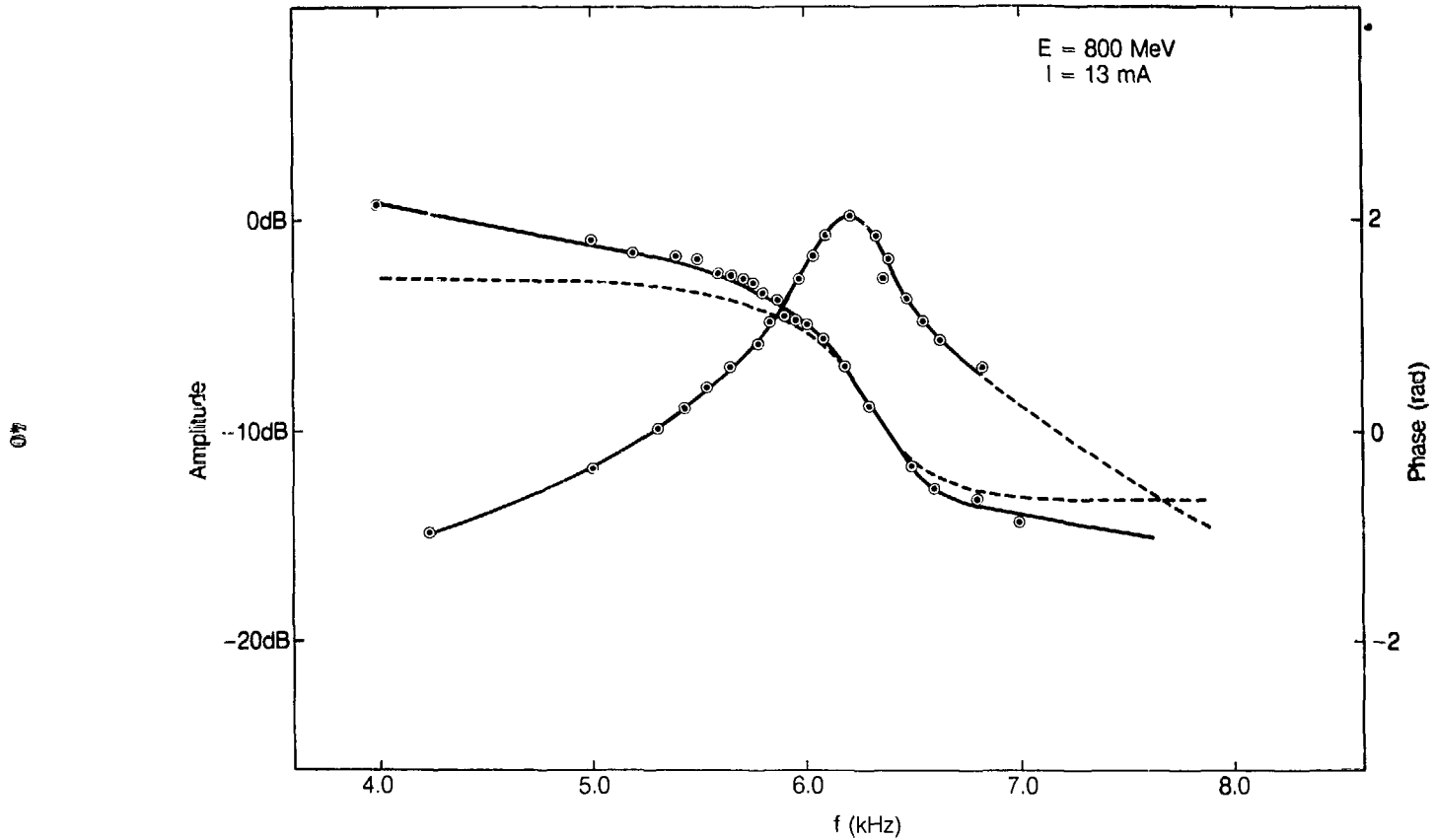
XBL 857-3075

Fig. 18 Phase and amplitude response from the longitudinal dipole mode transfer
function measurement at a beam intensity of 13 mA.
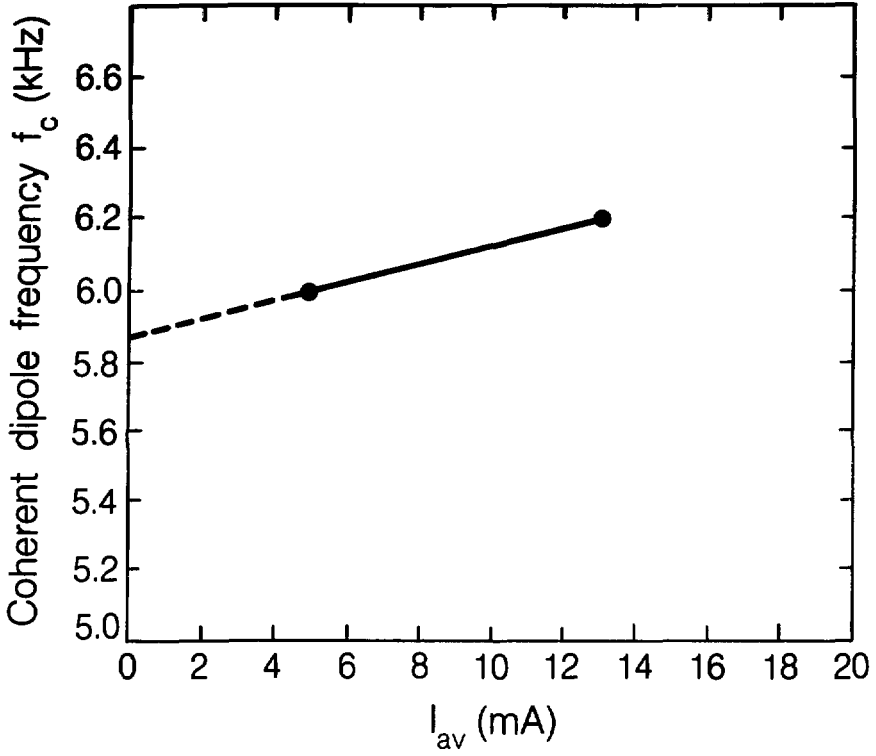
XBL 857-3071

Fig. 19 Coherent dipole mode frequencies, obtained from
Figs. 17 and 18, as a function of beam intensity.
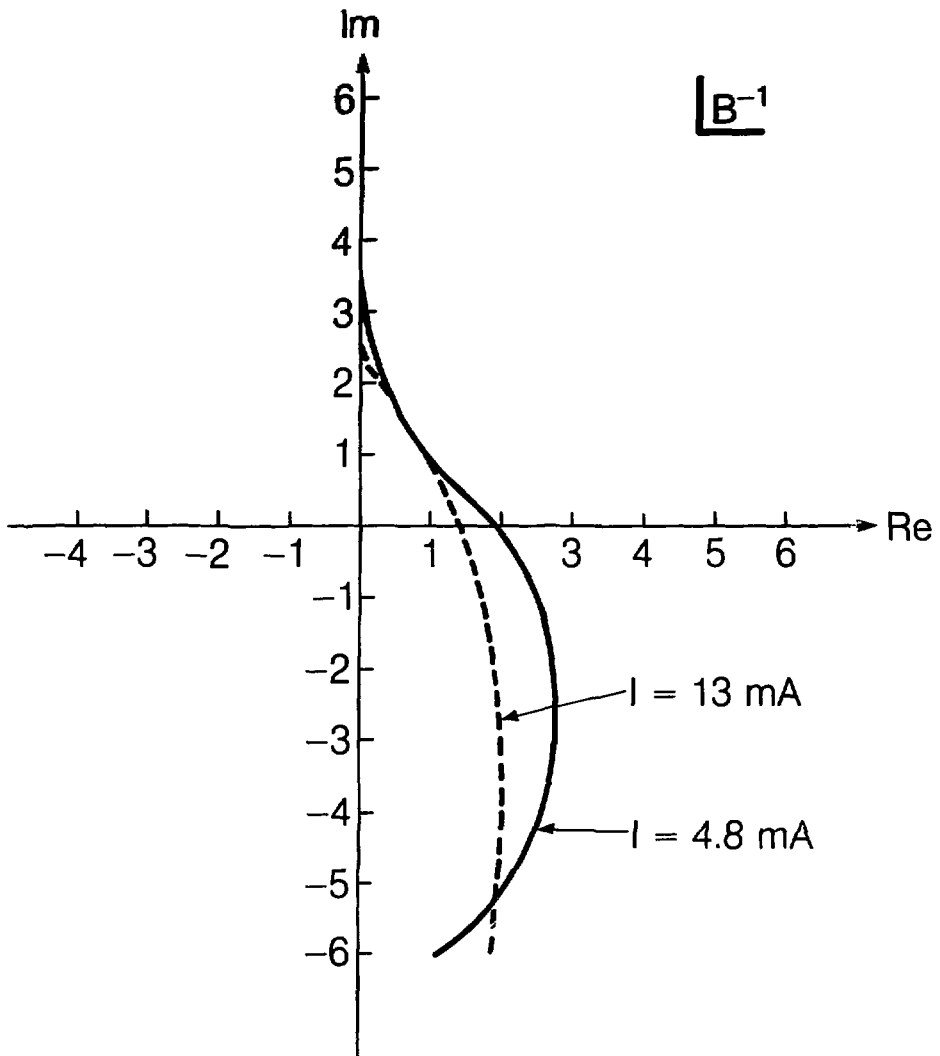
XBL 857-3070

Fig. 20 Stability diagrams for beam intensities of 4.8 mA
(solid curve) and 13 mA (dashed curve).
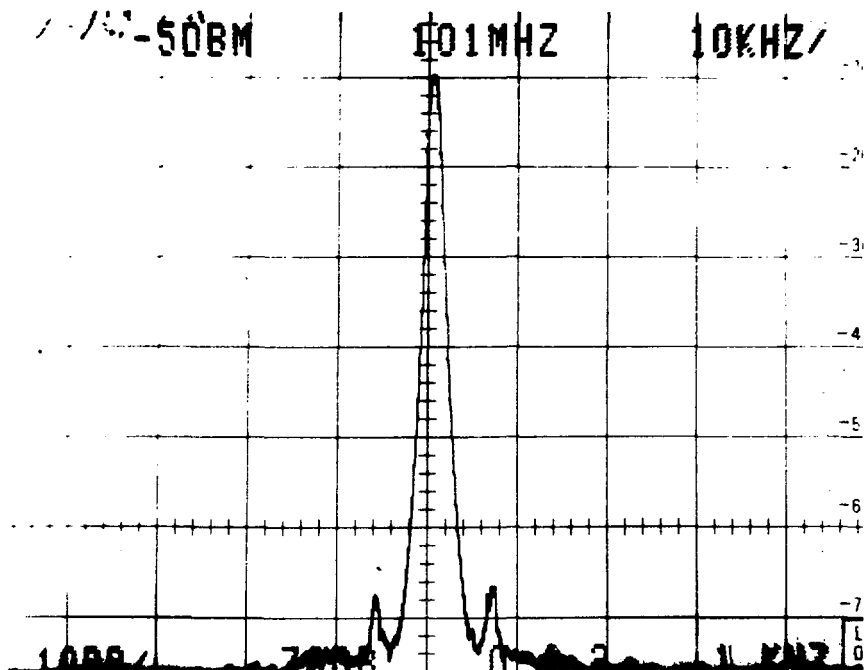
XBB 857-5189

Fig. 21 Spectrum analyzer trace around the second harmonic of the RF frequency, at 800 MeV and a beam intensity of 6.1 mA, showing synchrotron dipole oscillation side-bands.
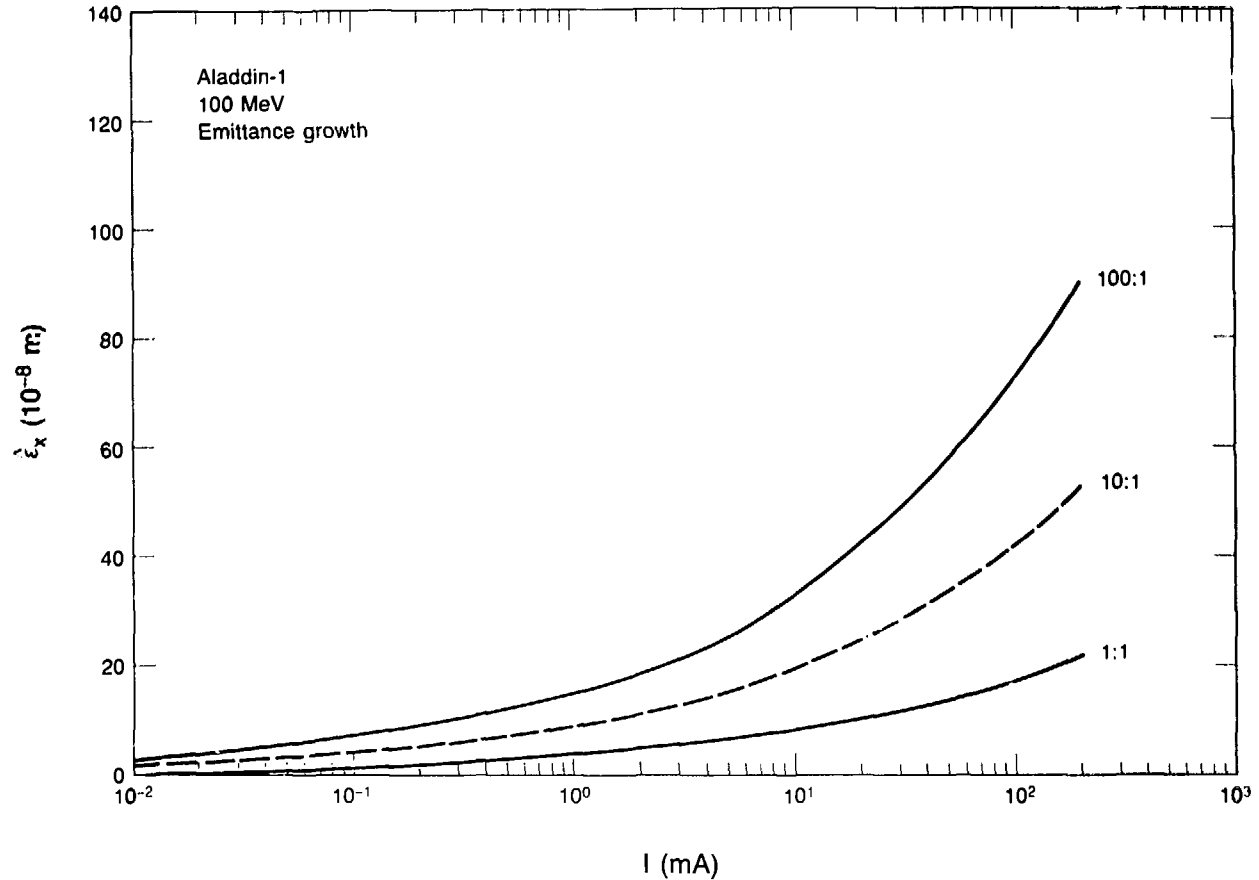
Fig. 22 Predicted equilibrium transverse emittance values (taken from Ref. 3), as
a function of beam intensity, based on IBS calculations. Three different
values for the horizontal-vertical emittance coupling are illustrated.
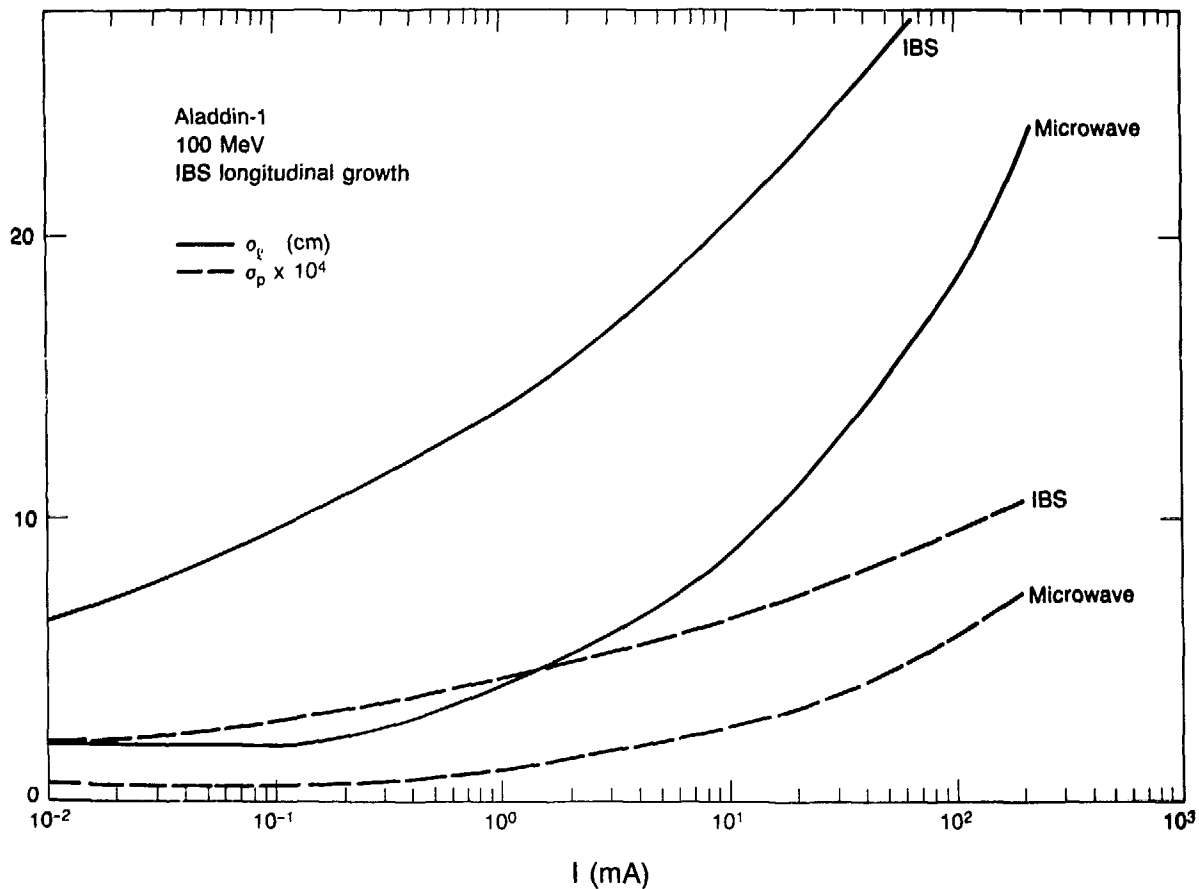
Fig. 23 Predicted equilibrium longitudinal bunch length and momentum spread
(taken from Ref. 3), as a function of beam intensity, based on IBS calcu-
lations.   Calculations based only on turbulent bunch lengthening from the
longitudinal microwave instability are shown for comparison.
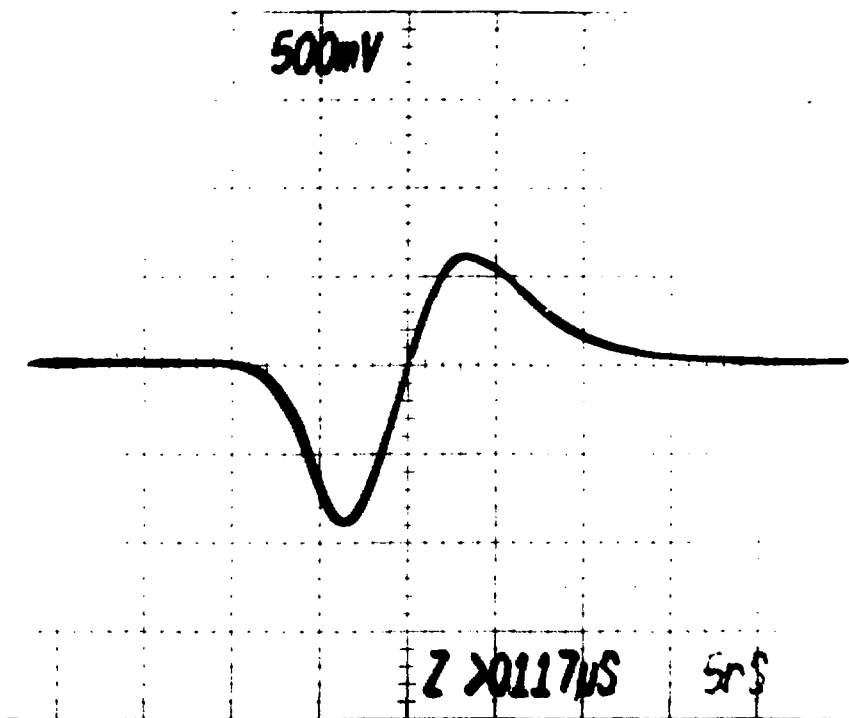
Fig. 24 Oscilloscope trace of bunch length profile from the
longitudinal pickup using the first-harmonic RF system.